

Three-halves harmonic emission from femtosecond laser produced plasmas with steep density gradients

L. Veisz, W. Theobald,^{a)} T. Feurer,^{b)} H. Schwoerer, I. Uschmann, O. Renner, and R. Sauerbrey

Institut für Optik und Quantenelektronik, Friedrich-Schiller-Universität, D-07743 Jena, Germany

(Received 11 April 2003; accepted 22 March 2004; published online 17 May 2004)

Detailed measurements of the angular distribution of $3\omega_0/2$ radiation are presented in short scale length plasmas ($0.8\text{--}7\ \mu\text{m}$) generated by laser radiation at intensities reaching the relativistic level ($10^{16}\text{--}6\times 10^{18}\ \text{W/cm}^2$). The experimental results are in very good agreement with theoretical predictions based on two-plasmon decay and stimulated Raman scattering instabilities. New three-halves harmonic generation mechanisms are an identified characteristic of femtosecond laser induced parametric instabilities. These are the joint interaction of incident and reflected laser beams as well as stimulated Raman scattering. It is shown both experimentally and theoretically that the three-halves harmonic radiation is a useful preplasma diagnostic tool. © 2004 American Institute of Physics. [DOI: 10.1063/1.1748174]

I. INTRODUCTION

Parametric instabilities are a very rich topic of laser-plasma interactions.¹ They have a basic impact on inertial confinement fusion, laser absorption, and propagation of light in plasmas, therefore, they were investigated in detail in the long pulse regime ($>100\ \text{ps}$).² Relevant instabilities involving the decay of the incident laser radiation, are stimulated Raman and Brillouin scattering (SRS and SBS) and two-plasmon decay (TPD). SRS (SBS) in plasmas is the decay of the laser electromagnetic wave into an electron plasma wave (ion acoustic wave) and another electromagnetic wave. TPD is the decay of an electromagnetic wave into two electron plasma waves and takes place in the vicinity of the quarter critical density. These plasma waves can couple with the incident laser light to generate $3\omega_0/2$ radiation, which was studied experimentally^{3–5} and theoretically.^{6–10}

After the introduction of chirped pulse amplification, see Ref. 11, ultrashort [sub-picosecond (ps)] table top terawatt lasers became available. Laser based fusion and especially the fast ignitor concept¹² led to a reinvestigation of some of the instabilities at higher intensities and shorter pulses.^{13,14} Particular attention was paid to SRS of ultrashort laser pulses, because SRS can affect the laser-based electron acceleration as well as drive the self-modulated laser wakefield acceleration.¹⁵ Processes that involve ion acoustic waves are generally suppressed due to the short time scales. Very little attention was paid to TPD although this instability is often present in femtosecond (fs)-laser-plasma experiments. It appears as bright colored light originating from the plasma. Using a Ti:sapphire laser with 800 nm central wavelength we first observed blue radiation as the intensity on target is in-

creased, which is the second harmonic radiation, then green radiation and at the highest intensity white light from the plasma. Although, several laboratories made similar observations see, for example, Ref. 16 so far this phenomenon has not yet been analyzed.

In this paper we present a study on the generation mechanisms of the three-halves harmonic radiation originating from the interaction of ultrashort, intense laser pulses with steep plasma gradients. In particular the angular distribution, as well as the intensity and scale length dependence of the emission are considered. We also compare our ultrashort pulse results with previous long pulse measurement and explain the different experimental scenarios. Spectral measurements support that the observed radiation is $3\omega_0/2$ emission with increasing bandwidth, which may be used as a simple preplasma diagnostic. In plasmas with a steep density gradient new types of $3\omega_0/2$ generation mechanisms become important with higher efficiency than the usual ones involving incident laser photon and TPD plasmon coupling. The first new mechanism is based on the joint interaction of the incident and reflected laser beams, which in the present geometry is possible only with intense ultrashort laser pulses and steep plasma gradients. The second new mechanism involves the SRS instability in the generation of three-halves harmonic radiation, which requires not only a prepulse-free, ultrashort, high intensity laser, but a carefully chosen experimental geometry.

Previously, the angular distribution was measured in the saturation dominated long laser pulse regime, which cannot be explained with the linear theory of unsaturated instability.⁴ For ultrashort laser pulses, however, the situation is different. The instability remains in or near the unsaturated regime.¹⁷ Therefore, it is expected that the experimental results are largely in agreement with the predictions of the linear model.

The paper is organized as follows. In Sec. II the theoretical description is outlined. The experimental setup is de-

^{a)}Present address: Center for Ultrafast Optical Science, University of Michigan, Ann Arbor, Michigan 48109-2099.

^{b)}Present address: Department of Chemistry, Massachusetts Institute of Technology, Cambridge, Massachusetts 02139.

scribed in Sec. III. The results are presented in Secs. IV and V and a detailed discussion of the results is found in Sec. V.

II. THEORY

In the present experiments the electron density scale length was below $10 \mu\text{m}$, typically $2\text{--}3 \mu\text{m}$, indicating that care must be taken in adopting the well known analytic models.^{6–9} Nevertheless, it is instructive to summarize the results of the previous works on three-halves harmonic generation and to complete them to describe the observations in the fs regime. The initial process in the $3\omega_0/2$ generation is the plasmon production with approximately $\omega_0/2$ frequency. We will investigate TPD and SRS as potential sources of these plasmons. Following these parametric instabilities, a coupling between a plasmon and a laser photon produces a new photon with $3\omega_0/2$ frequency.

We start the theoretical description of the earlier mentioned processes with the frequency and phase matching conditions, i.e., energy and momentum conservation, in the k space using the dispersion relations of the generated waves, similar to Meyer and Zhu.⁴ One should keep in mind, however, that frequency and phase matching alone is not sufficient to determine whether a $3\omega_0/2$ wave with detectable amplitude is generated. To complete the analysis, the growth rates in k space of the instabilities have to be considered. The k space analysis yields the wave vector of the generated $3\omega_0/2$ radiation, which determines the propagation direction and thus the angular distribution. Second, this analysis is a compact and illustrative form of the generation process. To start, we will restrict ourselves to the simplest model, i.e., resonant unsaturated parametric instabilities. Thereafter, we will complete the picture discussing additional effects, such as plasmon propagation or saturation.

The energy and momentum conservation for the TPD, SRS, and coupling process are

$$\omega_0 = \omega_{e_1} + \omega_{e_2}, \quad \mathbf{k}_0 = \mathbf{k}_{e_1} + \mathbf{k}_{e_2}, \quad (1)$$

$$\omega_0 = \omega_e + \omega_1, \quad \mathbf{k}_0 = \mathbf{k}_e + \mathbf{k}_1, \quad (2)$$

$$\omega_{3/2} = \omega_e + \omega_0, \quad \mathbf{k}_{3/2} = \mathbf{k}_e + \mathbf{k}_0, \quad (3)$$

where ω_j , \mathbf{k}_j ($j=0,1,3/2$) and ω_e , ω_{e_i} , \mathbf{k}_e , \mathbf{k}_{e_i} ($i=1,2$) are the frequency and wave vector of the electromagnetic waves and the electron plasma waves in the plasma, respectively. 0 refers to the laser, 1 to the scattered light by SRS, and 3/2 to the $3\omega_0/2$ light. We introduce here the normalized wave vectors $\tilde{\mathbf{k}} = kc/\omega_0$. The plasma supports eigenmodes of electromagnetic and plasma waves, which satisfy their dispersion relation. We note here that instabilities with large growth rate can generate waves which do not satisfy their dispersion relation, the instability is *nonresonant* in this case. The frequency of these nonresonant waves differs only slightly from those of the resonant waves and they have a smaller amplitude. The electromagnetic wave dispersion relation in plasma can be written as

$$\omega^2 = \omega_{pe}^2 + c^2k^2, \quad (4)$$

where c is the light speed in vacuum and $\omega_{pe} = \sqrt{e^2n_e/(\epsilon_0m_e)}$ is the local plasma frequency using e , n_e , and m_e the electron charge, density, and mass, respectively. For example the length of the laser wave vector at the quarter critical density is $k_0 = \sqrt{3}\omega_0/(2c)$. The plasma wave or plasmon dispersion relation is given by

$$\omega_e^2 = \omega_{pe}^2 + 3v_e^2k_e^2, \quad (5)$$

where $v_e = \sqrt{T_e/m_e}$ is the electron thermal speed and T_e is the average electron kinetic energy. We will denote the electron plasma temperature T_e in kilo-electron-volts with T . Since $3v_e^2k_e^2 \ll \omega_{pe}^2$ this is an optical-like dispersion relation, i.e., the frequency of the plasma wave depends weakly on its wave vector and $\omega_e \approx \omega_{pe}$. Consequently, the TPD instability takes place at the quarter critical density at low temperatures, where the critical density is $n_c = \epsilon_0m_e\omega_0^2/e^2$ or in practical units n_c (cm^{-3}) = $1.1 \times 10^{21}/\lambda_\mu^2$ and λ_μ is the wavelength of the laser in microns. SRS takes place at all densities up to the quarter critical density, but generates plasmons with $\omega_0/2$ energy that fulfill the energy conservation for $3\omega_0/2$ production only around $n_c/4$.

The laser beam is focused with an angle of incidence α onto an inhomogeneous plasma with a density scale length of $L = n_e/|\partial n_e/\partial x|$ at the quarter critical density. The direction of the density gradient is parallel to the x axis and the plane of incidence is the x - y plane.

The momentum conservation [Eq. (1)] restricts the TPD generated plasmon wave vectors to a sphere in k space at given plasma parameters (temperature and density). We limit the k space to a plane corresponding to the previous (horizontal) x - y plane, where the generated plasmon wave vectors are lying on a circle. Using Eqs. (1), (4), and (5) the plasmon wave vector generated by TPD at $n_c/4$ has to satisfy

$$\left[\tilde{k}_{ex} - \frac{\sqrt{\cos^2(\alpha) - 1/4}}{2} \right]^2 + \left[\tilde{k}_{ey} - \frac{\sin(\alpha)}{2} \right]^2 = \frac{\sqrt{n_e/n_c - 2n_e/n_c}}{3T/511} - \frac{3}{16}. \quad (6)$$

It can be seen from this equation that in fact TPD takes place below $n_c/4$ due to the finite electron temperature. Equation (6) is a circle centered at the normalized wave vector $\tilde{\mathbf{k}}_0/2$ with a radius that depends on T and n_e . The analytical expression obtained without these approximations deviates negligibly from this TPD circle, the difference is on the order of 1%. The plasmon wave vector is limited by the Landau damping in the case of TPD, as will be discussed later.

The k space analysis of the SRS is alike that of the TPD. However, similar assumption about the dispersion relations cannot be made, because the frequency of the scattered electromagnetic wave depends strongly on the wave vector. The SRS generated plasmon wave vectors satisfy

$$1 = \sqrt{\frac{n_e}{n_c} + \frac{3T}{511}(\tilde{k}_{ex}^2 + \tilde{k}_{ey}^2)} + \sqrt{\frac{n_e}{n_c} + \left[\tilde{k}_{ex} - \sqrt{\cos^2(\alpha) - \frac{n_e}{n_c}}\right]^2 + [\tilde{k}_{ey} - \sin(\alpha)]^2}. \tag{7}$$

Close to the quarter critical density this analytical curve is approximately a circle centered at the normalized wave vector $\tilde{\mathbf{k}}_0$ with a radius of $[1 - 2(n_e/n_c)^{1/2}]^{1/2}$. The scattered wave vector is negligible ($k_1 \ll k_0$) around the quarter critical density and consequently $\mathbf{k}_e \approx \mathbf{k}_0$.

Plasmons in the k space that can generate $3 \omega_0/2$ radiation, are determined basically by the momentum conservation of this process [Eqs. (3) and (4)]. The equation governing their wave vectors is

$$\left[\tilde{k}_{ex} + \sqrt{\cos^2(\alpha) - \frac{1}{4}}\right]^2 + [\tilde{k}_{ey} + \sin(\alpha)]^2 = 2. \tag{8}$$

This is the so called “*radiation circle*” centered at the normalized wave vector $-\tilde{\mathbf{k}}_0$ and with a radius of $\tilde{k}_{3/2} = \sqrt{2}$. Any deviation from the analytical expression is relative small. Only the radius covers a wide range of values corresponding to the three-halves harmonic bandwidth.

The propagation of the electromagnetic and plasma waves in inhomogeneous plasmas is easily illustrated in the k space. The perpendicular components of the wave vector with respect to the density gradient (y and z components) are conserved and only the parallel component (x) changes in order to satisfy the dispersion relation. Therefore, the propagation direction of the waves in k space is antiparallel to the density gradient. As the waves propagate inwards the electron density increases and the x component of the wave vector eventually vanishes. At this point the waves are reflected and the x component of their wave vector starts to grow again.

The propagation of light in the inhomogeneous plasma leads to reflection and for oblique incidence to refraction. In a plasma with a given density, the angle of refraction β is calculated using the dispersion relation [Eq. (4)] and keeping the perpendicular component of the wave vector constant. We find

$$\sin \beta = \frac{\sin \alpha}{\sqrt{\epsilon}} = \frac{\sin \alpha}{\sqrt{1 - \frac{\omega_{pe}^2}{\omega^2}}}, \tag{9}$$

where ω is the angular frequency of the light wave, α is the angle of incidence in vacuum, and ϵ is the dielectric function of the plasma. When the light wave is the incident laser we find $\omega_{pe}^2/\omega^2 = n_e/n_c$ and the density at the turning point is $n_c \cos^2(\alpha)$. The $3 \omega_0/2$ radiation, that is generated at the quarter critical density, will be subject to refraction and its wave vector and so the propagation direction will change slightly as it reaches the vacuum. The propagation of the laser light in the plasma is illustrated with the red curves in Fig. 1 in the normal space and also in the k space.

The plasmons propagate with a group velocity of $v_g = 3v_e^2 k_e / \omega_e$, which using the normalized wave vector for plasmons and a frequency of $\omega_e \approx \omega_0/2$ has the value $v_g = c\tilde{k}_e 6T/511$. The maximal distance that a plasmon propagates is restricted either by the collisional damping of plasmons or by the maximal length of the wave vector, which in turn is limited by the Landau damping of plasma waves with a long wave vector. The former is important in long pulse experiments and makes the plasma wave propagation and the change of the wave vector negligible, while the latter will be important in the ultrashort pulse experiments. We are interested in the plasmon propagation during the pulse duration, because $3 \omega_0/2$ is generated only during this time. While the frequency of the plasmon remains constant during propagation, the parallel component of the wave vector changes in a linear density profile according to Eq. (5):

$$\Delta \tilde{k}_{ex} = \tilde{k}_{ex} \left(\sqrt{\frac{\omega_0 \tau}{4\pi \tilde{k}_{ex} L/\lambda} + 1} - 1 \right), \tag{10}$$

where τ is the pulse duration, and L/λ is the density scale length normalized to the laser wavelength in vacuum.

To conclude the theoretical analysis we apply the formalism to a specific example of three-halves harmonic generation in the k space. We are able to predict the directions in which the $3 \omega_0/2$ radiation is generated, and moreover, their spectra. As mentioned previously, this analysis will be far from complete without taking into account the evolution of the first step of the $3 \omega_0/2$ production process, the parametric instabilities. The reason is that the initial exponential growth rates cause large variations in the amplitudes of plasma waves. Therefore, in some directions, which are in principle phase-matched, the three-halves harmonic radiation will have a negligible amplitude. Beyond that, the spectral shape is even more sensitive to the details of the instabilities.

We discuss in detail the TPD, which is an absolute instability growing exponentially in time as $\exp(\gamma t)$. The γ quantity is the growth rate and characterizes the instability. Waves with maximal growth rate, i.e., maximal amplitude

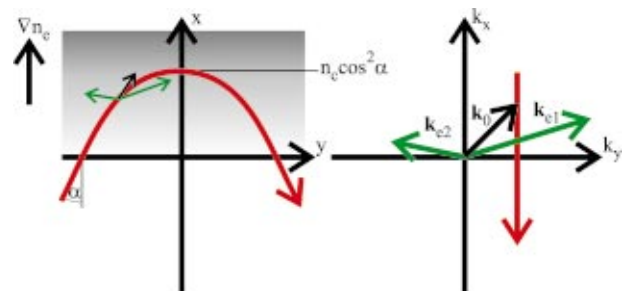


FIG. 1. (Color) Propagation of the laser light in the plasma (red lines) and the TPD in the normal space and in the k space. The black arrow is the laser wave vector, and the green arrows correspond to the plasma waves.

dominate the process and determine its properties. The plasma wave frequency is complex $\omega = \omega_r + i\gamma_0$, here ω_r is the real frequency of the plasma wave, in the resonant case $\omega_r = \omega_e$, and γ_0 is the growth rate in a homogeneous plasma. The TPD instability dispersion relation (Ref. 1)

$$(\omega^2 - \omega_{pe}^2 - 3v_e^2 k_e^2)[(\omega - \omega_0)^2 - \omega_{pe}^2 - 3v_e^2(\mathbf{k}_e - \mathbf{k}_0)^2] = \left[\frac{\mathbf{k}_e \mathbf{v}_{os}}{2} \omega_{pe} \frac{(\mathbf{k}_e - \mathbf{k}_0)^2 - k^2}{k_e |\mathbf{k}_e - \mathbf{k}_0|} \right]^2, \quad (11)$$

where $v_{os}/c = \sqrt{I\lambda^2/(1.37 \times 10^{18} \text{ W cm}^{-2} \mu\text{m}^2)}$ is the non-relativistic electron oscillation velocity in the laser field, and I is the laser intensity, care must be taken applying this at the highest intensities. This yields the growth rate

$$\gamma_0 = \frac{\mathbf{k}_e \mathbf{v}_{os}}{4} \left| \frac{(\mathbf{k}_e - \mathbf{k}_0)^2 - k_e^2}{k_e |\mathbf{k}_e - \mathbf{k}_0|} \right|. \quad (12)$$

We are interested in the value and properties of the maximum growth rate as discussed. We restrict ourselves to the case where \mathbf{k}_e is in the plane of \mathbf{v}_{os} and \mathbf{k}_0 since these plasma waves grow faster. A plasmon wave vector component perpendicular to the \mathbf{v}_{os} and \mathbf{k}_0 plane will appear only in the denominator of Eq. (12) thus diminishing the growth rate. The wave vectors of the plasmons having the maximum of this homogeneous TPD growth rate lie on the hyperbola

$$[\tilde{k}_{ex} \sin(\beta) + \tilde{k}_{ey} \cos(\beta)]^2 = [\tilde{k}_{ex} \cos(\beta) - \tilde{k}_{ey} \sin(\beta)] \times [\tilde{k}_{ex} \cos(\beta) - \tilde{k}_{ey} \sin(\beta) - \sqrt{3}/2]. \quad (13)$$

Here β is the previously calculated angle of incidence at the quarter critical density. This is the generalized form of the well known $k_{ey}^2 = k_{ex}(k_{ex} - k_0)$ maximum growth rate hyperbola for perpendicular incidence. This hyperbola and the wave vectors of the fastest growing plasmons point in the 45° direction between \mathbf{v}_{os} and \mathbf{k}_0 for large values of k_e . The value of the maximum growth rate along this hyperbola is $\gamma_{\max} = k_0 v_{os}/4$. We have to solve Eq. (11) numerically for the complex ω . The numerical solution also has its maximum along the hyperbola, but the maximum decreases with an increasing plasmon wave vector component perpendicular to \mathbf{k}_0 (k_{ey} in the following discussion). The TPD is illustrated in Fig. 1 in the normal and in the k space. The black arrow is the wave vector of the laser and the green ones correspond to the plasma waves. It should be noted that in this figure both the plasmons and the laser photons are plotted, later only the plasmon k space will be used.

There are several publications on the growth rate of TPD in an inhomogeneous plasma.⁶⁻⁹ Their results are valid in long electron density scale length plasmas ($L \gg 10 \mu\text{m}$), a condition that is strictly speaking not fulfilled in our experimental situation. Nevertheless, it is instructive to summarize the important points and deduce the physical consequences. The wave vector of the plasmon having maximum growth rate lies on the maximum growth rate hyperbola due to the homogeneous results, so the growth rate is only a function of the y component. Originally Liu and Rosenbluth⁶ calculated the growth rate of TPD in an inhomogeneous plasma as a

function of k_{ey} for perpendicular incidence, i.e., expanded the previous homogeneous growth rate with an inhomogeneous part. They derived the correct form of the inhomogeneous part, only the homogeneous portion was oversimplified. Lasinski and Langdon⁷ corrected the homogeneous growth rate by a term proportional to $-k_{ey}$. The correct form of the growth rate was first calculated by Simon *et al.*⁸ They calculated and simulated the growth rate and the TPD threshold condition in different parameter regimes. We focus onto our parameter range $1.41T^2/(I_{14}\lambda_\mu^2) \ll 1$ and $k_{ey} \sim k_0$, where $I_{14} = I/(10^{14} \text{ W/cm}^2)$. They obtained the TPD growth rate in inhomogeneous plasmas with linear density profile for perpendicular incidence as a function of k_{ey} along the maximum growth rate hyperbola (which determines k_{ex}):

$$\gamma(k_{ey}) = \frac{k_0 v_{os}}{4} - \frac{18v_e^4 k_0 k_{ey}^2}{v_{os} \omega_0^2} - \frac{\omega_0}{8k_{ey} L}. \quad (14)$$

This has a maximum value in practical units

$$\gamma_{\max}(\text{fs}^{-1}) = 3.47 \times 10^{-3} \sqrt{I_{14}} - 5 \frac{T^{2/3}}{\lambda_\mu^{4/3} (L/\lambda)^{2/3} I_{14}^{1/6}}. \quad (15)$$

The following threshold is obtained numerically:

$$\frac{v_{os}^2}{4v_e^2} k_0 L = 0.0504 \frac{L_\mu \lambda_\mu I_{14}}{T} > 3.1, \quad (16)$$

where L_μ is the scale length in microns, the constant 3.1 slightly deviates from the analytical value (2.8) derived from Eq. (15).

Afeyan and Williams⁹ reinvestigated the problem exhaustively in oblique incidence with p and s polarization. They obtained the same results as Simon *et al.* under similar conditions. In the case of oblique incidence, s polarization and a linear density profile, the nominal scale length (L) is smaller than the effective scale length in the \mathbf{v}_{os} and \mathbf{k}_0 plane, $L_{\text{eff}} = L/\cos(\beta)$. The increased scale length is compensated by the decreased intensity due to the enlarged focus spot in oblique incidence so the threshold will not change [Eq. (16)], although above threshold this yields a slightly slower growth. The situation is more complex for p polarization. Here the effective scale length depends on the propagation direction of the plasmon. The threshold depends on the fact in which arm of the maximum growth rate hyperbola the plasma wave is located and can be higher than for perpendicular incidence. The theory suggests that the growth rate far above threshold is not affected by the inhomogeneity and slightly slower than for perpendicular incidence.

There are two important effects of the inhomogeneity on the TPD which are valid for small density scale length also. First, the propagation of the plasma wave leads to a rapid change of its wave vector due to the high dispersion. Therefore, the plasma wave propagates away from the maximum growth area in the k space and switches off the instability. Practically, the plasmon generated on the maximum growth rate hyperbola propagates and leaves the hyperbola. Second,

the more the plasma density changes within a plasmon wavelength the harder the generation of a plasmon. This is suggested by the inhomogeneous part of the growth rate in Eq. (14).

The SRS instability was thoroughly investigated theoretically in homogeneous^{1,18} and inhomogeneous plasmas.^{19,20} It takes place in a wide range of densities up to quarter critical. The growth rate has been calculated in different situations depending on the direction of the scattered electromagnetic radiation, i.e., in back, side, and forward direction. We restrict ourselves to scattering in the plane of polarization, because our measurements were performed in this plane. The SRS backscattering growth rate in a homogeneous plasma

$$\gamma_{\text{SRS}} = \frac{k_e v_{\text{os}}}{4} \left(\frac{\omega_{\text{pe}}^2}{\omega_e(\omega_0 - \omega_e)} \right)^{1/2}, \quad (17)$$

where the plasmon wave vector $k_e = k_0 + \omega_0/c(1 - 2\omega_{\text{pe}}/\omega_0)^{1/2}$ which reaches k_0 around quarter critical density, where the growth rate is maximal and has a value of $k_0 v_{\text{os}}/4$ similar to TPD. Side scattering in the plane of polarization has a lower growth rate.

It is important to mention that around the quarter critical density SRS and TPD can share the same plasma waves. The growth of the instabilities depends, among others, on the amplitude of the daughter waves. The amplitude of the shared wave is certainly higher in this case, which leads to a boost in the growth of both instabilities. Afeyan and Williams elaborated the previous situation and called this high frequency hybrid instability,²¹ but others have also identified it at relativistic intensities.^{22,23} As we will see this can contribute to our results due to the plasmon propagation.

Parametric instabilities certainly do not grow unlimited, because different processes such as coupling to other waves, pump depletion, or plasma wave breaking limit the amplitude of their daughter waves. Langmuir wave decay instability (LDI) is a decay of a plasma wave into another scattered plasma wave and an ion acoustic wave. LDI was identified as the nonlinear saturation mechanism of the TPD in the long pulse regime.¹⁰ In these experiments LDI had another very important role, it produced plasmons with “new” wave vectors, that were not produced by TPD and these plasmons could couple with the laser to generate $3\omega_0/2$. This is the main three-halves harmonic generation process in the nanosecond (ns) regime. This process requires the generation of ion acoustic waves with some ps cycle time, which are generally suppressed in the fs regime. Consequently, we expect the same or higher saturation amplitude than for long pulses. An amplification of the plasma wave intensity of 7–9 e foldings ($10^3 - 10^4$) was measured,²⁴ which is a lower limit in the short pulse regime. Pump depletion does not play a role, because the three-halves harmonic energy is low enough to assume a negligible amount of energy in the plasma waves. Other processes involving only electromagnetic and plasma waves as well as wave breaking are possible candidates as saturation mechanisms in short pulse experiments.

Furthermore, instabilities generated by a long or a short pulse laser with the same fluence have absolute different be-

havior. The amplification depends on the fluence ($F = I\tau$ in the case of a rectangular pulse) and the pulse duration (τ), in e foldings $\gamma_{\text{max}}\tau \sim \sqrt{I}\tau = \sqrt{F}\tau$. This estimate implies a factor of 100 less amplification with a 100 fs than with a 1 ns laser. Taking into account that a linear growth lasts 10–20 ps,⁴ approximately 1% of the pulse duration with ns lasers, we expect a predominantly exponential growth for fs pulses.

We discuss briefly the loss mechanisms of the electromagnetic and the electrostatic waves. Resonance absorption of light in a plasma is an important process that can decrease the energy of light significantly in the case of p polarized and obliquely incident waves.¹ This is a direct generation of a plasmon by a photon, that tunneled to the critical density to fulfill the matching conditions. A longitudinal plasma wave is generated by the light electric field component perpendicular to the plasma surface. The maximum absorption can reach 50% in the angle

$$\sin(\alpha_{\text{ra}}) = \frac{0.8}{(2\pi L/\lambda)^{(1/3)}}, \quad (18)$$

where α_{ra} is the angle of incidence in vacuum at which the resonance absorption is maximized. The absorption is sizeable in the $\Delta\alpha_{\text{ra}} \sim \alpha_{\text{ra}}$ incidence angle range.

Collisions between electrons that oscillate in the electric field of a light wave and ions represent a loss for the light wave. This collisional absorption is not significant in high intensity experiments ($I > 10^{15}$ W/cm²) due to the decreased electron-ion collision frequency, the higher plasma temperature and the smaller interaction length.

We consider the collisional and the Landau damping as plasma wave damping mechanisms. In both cases the previously calculated instability growth rate is diminished by a corresponding term. The collisional damping has a temporal damping rate at the quarter critical density of

$$\gamma_{\text{coll}} = \frac{\omega_{\text{pe}}^2}{2\omega_e^2} \nu_{\text{ei}} \approx 8.8 \times 10^{-5} \frac{Z}{\lambda_{\mu}^2 T^{3/2}} \text{ fs}^{-1}, \quad (19)$$

where ν_{ei} is the electron ion collisional frequency and Z is the ionization charge state.

The Landau damping is an important loss mechanism of electron plasma waves.¹ We treat this either as negligible or as dominant, in which case the plasmon is heavily damped. An easy estimation of the sizeable Landau damping $k_e \lambda_{\text{De}} \geq 0.3$ where $\lambda_{\text{De}} = \sqrt{T_e/(4\pi n_e e^2)}$ is the Debye length, in useful units $\tilde{k}_e \geq 3.4/\sqrt{T}$. The complete Landau damping coefficient is

$$\gamma_L \approx \frac{857.3}{\lambda_{\mu} \tilde{k}_e^3 T^{3/2}} \exp\left(-\frac{63.88}{\tilde{k}_e^2 T}\right) \text{ fs}^{-1}. \quad (20)$$

III. EXPERIMENTAL SETUP

In the last section the theoretical aspects of $3\omega_0/2$ generation were summarized. Measuring the angular distribution and the dependencies of this distribution on various parameters such as intensity or scale length the experimental results may be compared with this theory. Now, we focus on

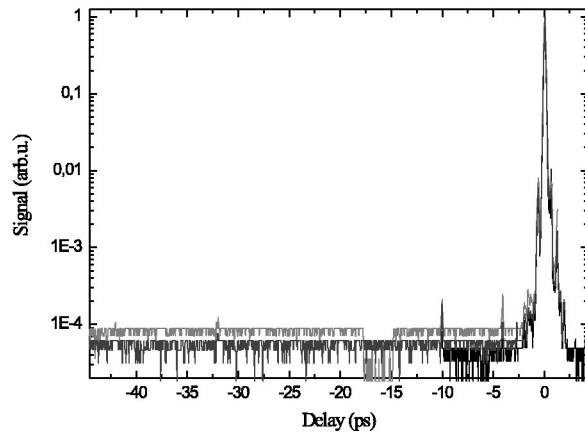


FIG. 2. Three third harmonic generation autocorrelations with a dynamic range of better than four orders of magnitude. Two 100 fs prepulses are detected at 10 and 4 ps.

these experimental observations. The Ti:sapphire laser had a central wavelength of 800 nm, a bandwidth of 14 nm, a pulse duration of $94 \text{ fs} \pm 5\%$ [full width at half maximum (FWHM) pulse duration assuming a Gaussian pulse], and p polarization. The energy on target varied between 155 and 175 mJ with a relative standard deviation of $\pm 4\%$. The pulse compressor was installed in a vacuum chamber to avoid nonlinear effects in the air. Two approximately 100 fs long prepulses were detected 10 and 4 ps before the main pulse. The intensity contrast with respect to the main pulse was measured to 2×10^{-4} using a third order, high dynamic range autocorrelator (see Fig. 2). An additional prepulse was introduced with the same pulse duration using a prepulse generator,²⁵ which contained 2% of the energy of the main pulse. The delay of the prepulse was changed between 0 and 350 ps. A regular control of the focal intensity distribution indicated a FWHM focus diameter of $2.9 \mu\text{m} \pm 0.3 \mu\text{m}$ (containing 43% of the energy on target) and independently a Rayleigh range of $21 \mu\text{m} \pm 3 \mu\text{m}$ by measuring the transverse intensity distribution in front of and after the focus in several positions. An angle of incidence of 45° leading to a slightly increased spot size in one dimension caused a decrease of the intensity on target. The average intensity within the temporal and spatial FWHM on target including the previous effects was $(6.2 \pm 1.2) \times 10^{18} \text{ W/cm}^2$ in the focus. The temporal and spatial peak intensity is 1.72 times higher, that is $(1.1 \pm 0.2) \times 10^{19} \text{ W/cm}^2$. The intensity was varied by moving the target along the optical axis out of the focus. As compared to decreasing the energy this method has the advantage that the signal to noise ratio of the detected $3 \omega_0/2$ radiation was much larger. A disadvantage of changing the target position is that the angle of incidence will change to an angular range instead of a well defined value. We will show in this article that the power and the direction of the emission depend on, amongst other things, the angle of incidence therefore this angular range must be taken into account.

Aluminum targets on glass substrates were used in the experiments. The pressure was typically 7×10^{-5} mbar in the vacuum chamber. The horizontal plane of the geometry is depicted in Fig. 3. The direction normal to the target surface

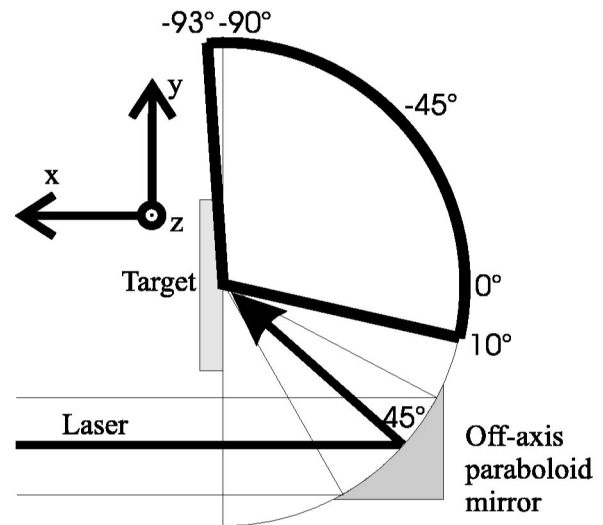


FIG. 3. Geometry of the measurement and the definition of the angles.

in the horizontal plane is defined as 0° . The angle of incidence and the specular reflection angle were 45° and -45° , respectively. The angular range between 10° and -93° was scanned. The laser was focused with an off-axis paraboloid gold mirror and the $f/3.4$ focusing yielded an angular width of 16° in the horizontal direction.

X-ray spectral measurements²⁶ were performed at various intensities to determine the electron plasma temperature. The obtained spectra were simulated with known parameters. In the intensity regime used here the best fit yielded an electron temperature of 1.05 keV at $5 \times 10^{23} \text{ cm}^{-3}$ density. The variation of the temperature with the intensity was less than 15%. Although, the measured plasma density is much higher than the quarter critical density ($4 \times 10^{20} \text{ cm}^{-3}$) we assume a similar temperature there, because their spatial distance is approximately $10 \mu\text{m}$ and the plasma temperature varies much slower than the density.²⁷

IV. 3 $\omega_0/2$ SIGNAL DEPENDENCE ON THE SCALE LENGTH

The $3 \omega_0/2$ signal dependence on the main pulse-prepulse delay, i.e., on the scale length (L) at the quarter critical density of the preplasma, was measured in order to determine the maximum $3 \omega_0/2$ yield. The electron density scale lengths for the various main pulse prepulse delays in Fig. 4 were calculated by the 1D MEDUSA code.²⁸ The simulations were compared to experimental results obtained under similar conditions in Ref. 29 and the results indicate that the one-dimensional code simulating the plasma expansion is appropriate. For all delays applied the scale length is smaller than $7 \mu\text{m}$.

The plasma radiation was directed through a vacuum window, spectrally filtered with care and the three-halves harmonic content was measured with a photodiode in -15° observation angle. The intensity on target was $(7 \pm 3) \times 10^{16} \text{ W/cm}^2$. The result is shown in Fig. 4. First, the signal increases rapidly with scale length, reaches a maximum at around 50 ps, and decreases again after 100 ps. A similar

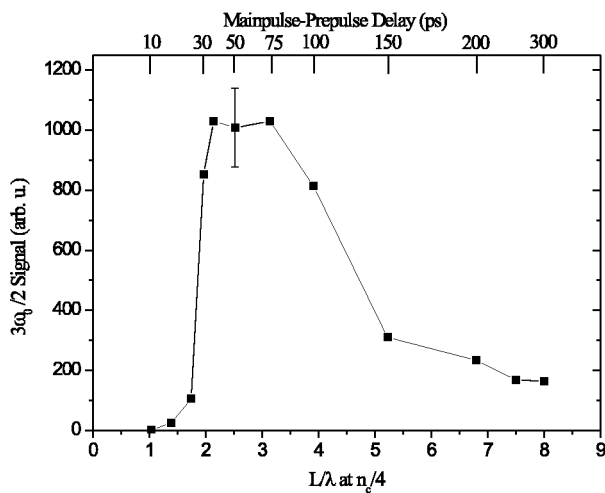


FIG. 4. Change of the $3\omega_0/2$ signal with the scale length at $I = 7 \times 10^{16}$ W/cm² for an observation angle of -15° .

behavior is observed in other directions (-24° , -67°). Only in 0° direction a deviation is found, here, the rapid increase is followed by a slow growth and no pronounced maximum is observed (Fig. 5).

Previous investigations have shown that the $3\omega_0/2$ photons are produced in a nonlinear interaction between a fundamental laser photon and a plasmon, where the plasmon was generated by TPD,¹⁷ as was suggested originally by Barr.³⁰ The spatial region along the density gradient where $3\omega_0/2$ radiation is generated, i.e., the *active region*, depends on the electron plasma temperature.³¹ For the present experimental conditions a plasma temperature of about 1 keV and an active region from approximately $0.2n_c$ to $0.25n_c$ is estimated. We expect an increasing signal with increasing scale length as the inhomogeneous part in the growth rate decreases in Eqs. (14) and (15), but the change in the measured signal between $L/\lambda = 1$ and 2 is more dramatic than predicted by the exponentiated maximum growth rate multiplied with the pulse duration as the interaction time. Another discrepancy is found by calculating the threshold intensities at a

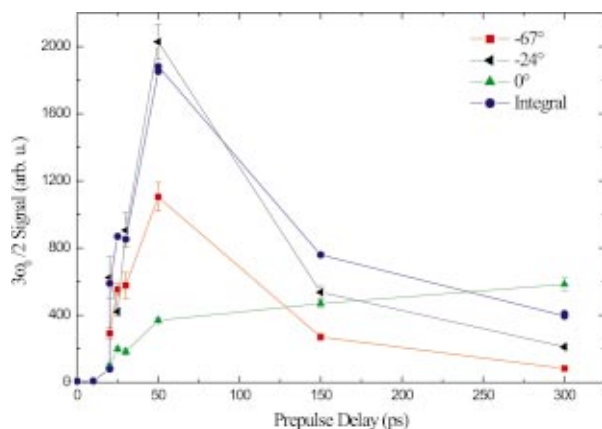


FIG. 5. (Color) Change of the $3\omega_0/2$ signal with the delay between the main pulse and the prepulse at $I = 7 \times 10^{16}$ W/cm² for observation angles of -67° , -24° , 0° , and the integral of the angle distributions from -90° to 10° .

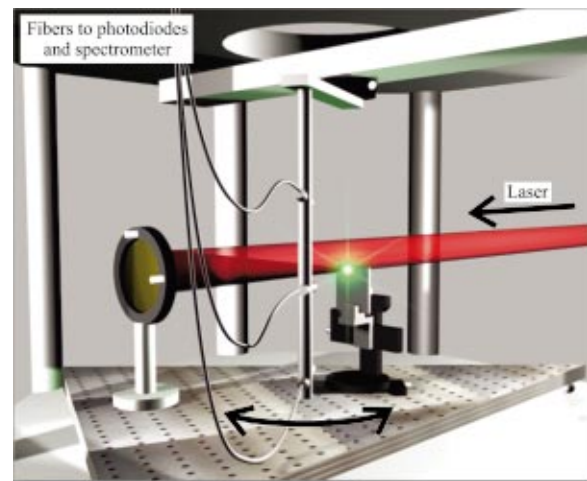


FIG. 6. (Color) Setup of the angle distribution measurement.

given short scale length. The threshold from Fig. 4 at about a normalized scale length of $L/\lambda \sim 1 - 1.25$ is 7×10^{16} W/cm², while from Eq. (16) we obtain $7 - 9 \times 10^{15}$ W/cm². Almost one order of magnitude smaller than the experimental value so we conclude that other effects start to play a more dominant role. The measured signal cannot be explained even if we take into account saturation effects and the start of absorption mechanisms at ultra short scale length. Although, the plasmon propagation reduces the signal at small scale length more than by longer ones due to the already discussed propagation away from the large growth rate regions in the k space, so drastic change in the signal as measured is not expected from this effect.

One possible explanation is based on the fact that no $3\omega_0/2$ radiation is generated as long as the active region is smaller than the wavelength of the plasmons. The plasmon wavelength for the present conditions is between 500 nm and $1 \mu\text{m}$. This wavelength is estimated from the length of plasmon wave vector for plasma waves that have a significant growth rate and can generate $3\omega_0/2$. For the present conditions we find $k \sim 1 - 2 k_0$, where k_0 is the wave vector of the incident laser at the quarter critical density. Once the active region becomes comparable to the wavelength of a plasmon the exponential growth of the instability leads to a detectable signal level. This supports the well known experimental observations that the $3\omega_0/2$ light is a sign for a preplasma. Furthermore, the previous explanation implies that the presence of $3\omega_0/2$ radiation in high intensity experiments indicates a preplasma with a scale length of about λ or higher. Accordingly, the three-halves harmonic, which is optically very easily detected by typical laser wavelengths, can be used as a simple preplasma diagnostic tool. As the scale length increases other effects, such as the change of the plasma geometry and saturation of the growth rate, become important.

V. $3\omega_0/2$ ANGULAR DISTRIBUTION

A. Experimental results

To measure the angular distribution of the $3\omega_0/2$ radiation the setup shown in Fig. 6 was used. The plasma emis-

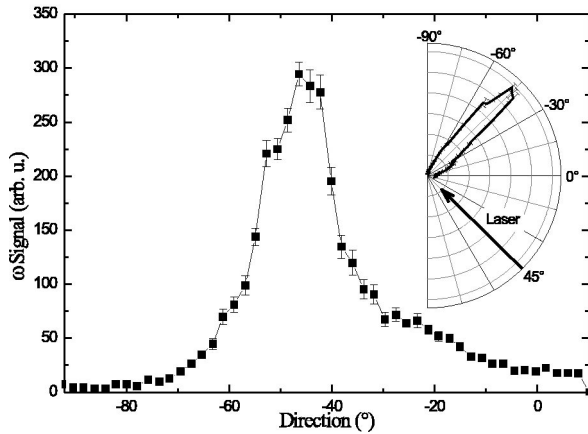


FIG. 7. Angular distribution of the reflected laser pulse with $I=6 \times 10^{18}$ W/cm² and 50 ps prepulse. Inset: polar plot with the incident laser direction.

sion was guided out of the vacuum chamber by three 1 mm thick and 3 m long optical quartz fibers. After proper spectral filtering three photodiodes measured either the $3\omega_0/2$ signal, or the second harmonic signal, or the fundamental light. In the -15° direction the different signals from the plasma were measured directly through a vacuum window.

The middle fiber was placed in the plane of incidence, its distance from the plasma was 190 mm and it collected light within an angle of 0.3° . The upper and lower fibers were placed at an angle of $30^\circ \pm 3^\circ$ with respect to the horizontal plane. All data points in the angular distribution measurements were averaged over 10–100 laser shots depending on the measurement series, and the error bars denote the calculated statistical errors.

The measured angular distribution of the reflected fundamental laser light in the plane of incidence at an intensity of 6×10^{18} W/cm² is shown in Fig. 7. The angular spread around the peak at $-45^\circ \pm 1^\circ$ is $16^\circ \pm 1^\circ$ which reflects exactly the divergence of the focused laser beam. There is an important consequence of the tight focusing as discussed earlier, that is, if the target is not in focus the angle of incidence is not a well defined value but varies across the beam in the transverse direction ($45^\circ \pm 8^\circ$). In some cases this will cause a smearing of the measured features.

A typical $3\omega_0/2$ angle distribution for an intensity of 7×10^{16} W/cm² is shown in Fig. 8. A 20 ps prepulse was applied and the scale length just barely exceeds the threshold. Under these conditions the $3\omega_0/2$ emission was very weak and showed high fluctuations which is a typical feature of the linear regime close to the threshold (exponential growth). The results show that the signal is peaked around the two angles $-28^\circ \pm 3^\circ$ and $-71^\circ \pm 3^\circ$. The error bars are relatively large due to the large fluctuations close to threshold. Recently, other groups made similar experimental observations of the double-peaked angular distribution.³²

At a delay of 50 ps, where the $3\omega_0/2$ yield is maximal, the angle dependent signal is shown in Fig. 9. The intensity was slightly higher, namely 1.3×10^{17} W/cm². Again a double-peak distribution is found and the peaks are located at the same values as in Fig. 8. Two independent measurements

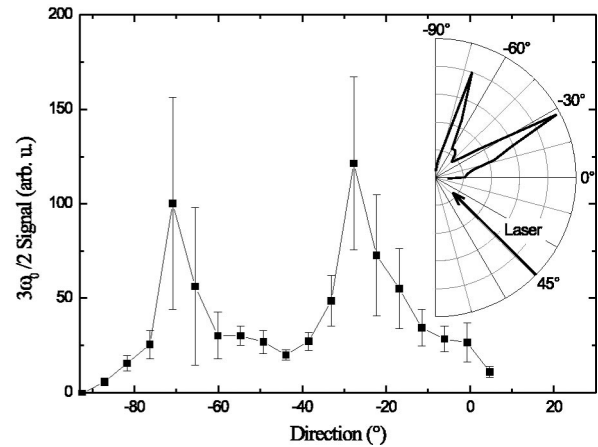


FIG. 8. $3\omega_0/2$ angular distribution with 20 ps prepulse and 7×10^{16} W/cm² intensity. Inset: polar plot with the incident laser direction.

are plotted in Fig. 9 to demonstrate that well above the threshold the reproducibility was very good. Fitting the data to two Gauss functions allows to estimate the widths and the relative amplitudes of the two maxima. The first higher peak is at about $-26^\circ \pm 3^\circ$ and has a FWHM of 30° and the second peak is at $-67^\circ \pm 3^\circ$ with a FWHM of 15° . The widths have been deconvoluted with the angular spread of the incident laser beam. The diodes connected to the upper and lower fibers recorded similar angle distributions as the center diode, but the characteristic peaks were not as pronounced.

In summary, the $3\omega_0/2$ spectra show a very pronounced double-peaked structure. The detailed spectral features depend on the prepulse-main pulse delay, i.e., the scale length. To investigate the previous results in greater detail the scale length, i.e., the size of the inhomogeneous plasma, and the intensity were varied.

B. Angular distribution for various scale lengths

The angular distributions for different scale lengths at a nonrelativistic intensity of $(1.3 \pm 0.5) \times 10^{17}$ W/cm² are depicted in Fig. 10. The double-peak structure is observed for

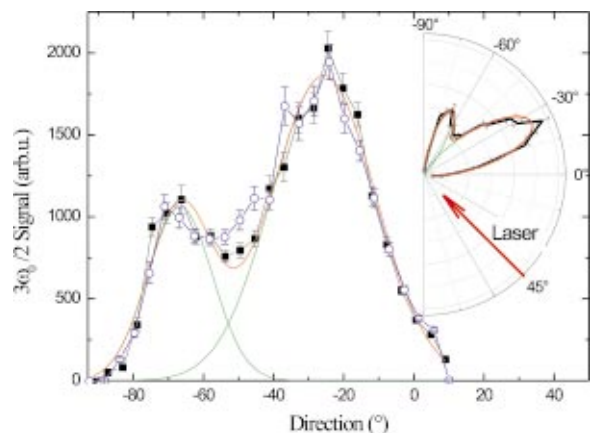


FIG. 9. (Color) Two independently measured $3\omega_0/2$ angle distributions with 50 ps prepulse and 1.3×10^{17} W/cm² intensity. The solid lines are Gaussian fits to the peaks. Inset: polar plot with the incident laser direction.

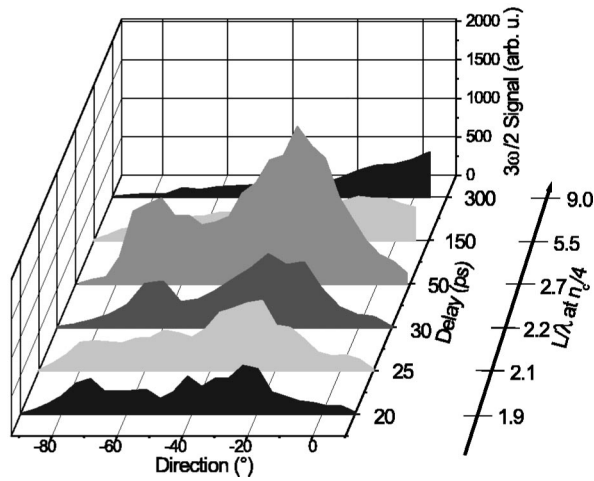


FIG. 10. $3\omega_0/2$ angular distributions with different main pulse-prepulse delays and 1.3×10^{17} W/cm² intensity. Increasing signal with double-peaked structure is observed with delays <100 ps, while the double-peaked structure disappears and the signal decreases for longer delays.

prepulse-main pulse delays smaller than about 100 ps. This corresponds to the range in Fig. 4 where the signal is either growing or constant. At larger delays and consequently at larger scale lengths the peaks disappear, this starts at $L/\lambda \sim 5$. It is important to note that the three-halves harmonic signal decreases significantly with the change of the angular distribution.

C. Angular distribution for various intensities

Figure 11 shows angular distributions for different intensities at a 50 ps prepulse-main pulse delay. The intensity was varied by moving the target along the optical axis as depicted on the right side of Fig. 11. Accordingly, the intensity scale has its maximum in the middle of the axis and decreases in both directions, which corresponds to a target position in front of or behind the focus. Note that the scale length increases weakly with the intensity. For the lowest intensities

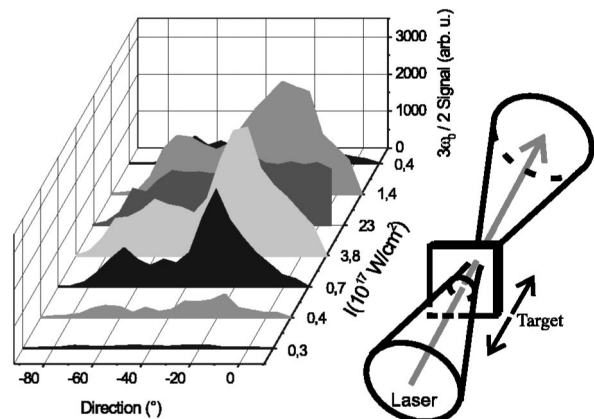


FIG. 11. $3\omega_0/2$ angular distributions with different intensities and a 50 ps prepulse. The small picture on the right depicts how was the intensity changed. Correspondingly the intensity axis has its maximum in the middle. The double-peaked structure disappears at the highest intensity.

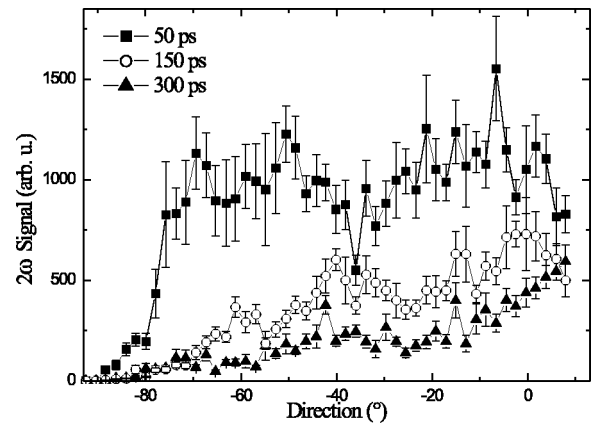


FIG. 12. $2\omega_0$ angular distributions with an intensity of 6×10^{18} W/cm². The curve with the squares represents the measurement with a 50 ps prepulse, the circles a 150 ps prepulse, and the triangles a 300 ps prepulse.

almost no $3\omega_0/2$ emission is detected. At intensities which reach the relativistic level the observed double-peak structure disappears.

The TPD instability exhibits a threshold intensity at which the growth rate becomes positive and which was discussed in Eq. (16). This condition yields a threshold intensity of 6×10^{15} W/cm² (Ref. 8) (assuming $T_e = 1$ keV and $L/\lambda = 1.6$). The measured threshold intensity in Fig. 11 is $(2 \pm 1) \times 10^{16}$ W/cm², and therefore, about 2–3 times higher than the calculated value. Comparing this discrepancy with the previous one, we see that the difference between theory and measurement is smaller at a slightly longer scale length. This supports the statement that the inhomogeneous growth rate loses its validity around $L/\lambda \approx 1$. The double-peaked structure is observed above the threshold up to an intensity of about 2×10^{18} W/cm². At this intensity the scale length is approximately 6 μm and the structure disappears similar to the results shown in Fig. 10.

Measurements of the $2\omega_0$ angular distribution show that the second harmonic radiation is also isotropic for scale lengths at ~ 7 μm. The results are shown in Fig. 12 for an intensity of $(6 \pm 1) \times 10^{18}$ W/cm² and a prepulse main pulse delay of 50, 150, and 300 ps, respectively. The $2\omega_0$ signal decreases with increasing scale length. For the highest scale length the second harmonic radiation peaks in the $10^\circ \leftrightarrow 90^\circ$ range direction very similar to the $3\omega_0/2$ results. Therefore, it is assumed that the disappearance of the double-peak structure is a consequence of spatial effects, for example hole boring, that affect all radiation and are not specific to the $3\omega_0/2$ radiation.

VI. DISCUSSION OF THE ANGULAR DISTRIBUTION

To calculate the $3\omega_0/2$ scattering angle a k space analysis, introduced in the theory section, was performed. As mentioned earlier, the most probable $3\omega_0/2$ generation process is the coupling of a laser photon to a plasmon and the electron plasma wave is generated by the TPD. In Figs. 13 and 14 the k_x axis is parallel to the direction of the density gradient as earlier.

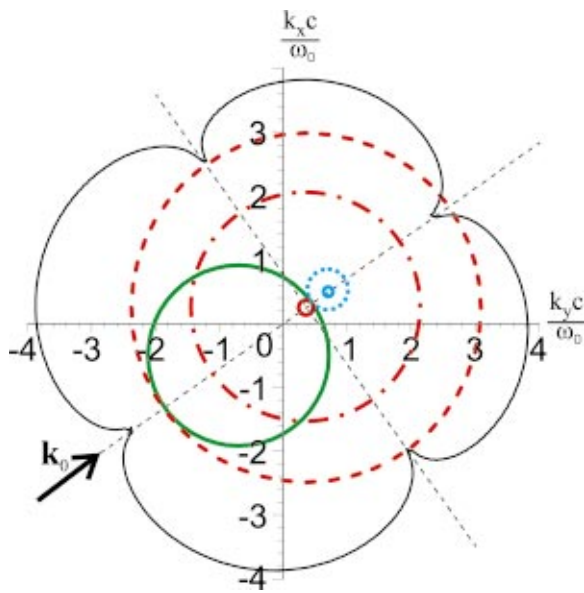


FIG. 13. (Color) k space analysis of the instabilities. The thin dotted axes are the axes of a new coordinate system at the quarter critical adapted for the case of 45° incidence angle. Note that due to refraction the laser wave vector at $n_c/4$ (\mathbf{k}_0) is inclined by an angle of 55° with respect to the k_x axis, which is parallel with the electron density gradient. The Landau damping is equal to the homogeneous growth rate on the thin clover-leaf-shaped curve at 10^{17} W/cm 2 . Plasma waves with wave vectors on the thick green radiation circle can generate $3\omega_0/2$ with the incident laser. The thick red curves are TPD circles for three electron densities. The small solid circle is for an electron density of about $0.25n_c$, the middle dashed-dotted circle for $0.23n_c$ while the larger dashed circle about $0.2n_c$ at 1 keV. The light blue curves are SRS generated plasma waves at $0.245n_c$ (smaller) and $0.2n_c$ (larger).

For a given electron plasma temperature and electron density the tip of the plasmon wave vector generated by TPD is located on a circle, Eq. (6). The radius of the TPD circle depends strongly on the electron density and the wave vectors of plasma waves generated through TPD lie on the larger red dashed circle in Fig. 13 at approximately $0.2n_c$ (at 1 keV), on the middle dashed-dotted circle at $0.23n_c$ and on the smaller red solid circle at slightly less than $0.25n_c$. The $3\omega_0/2$ photon is born on the green radiation circle, which is described by Eq. (8). The radiation circle hardly changes in the considered electron density range. There are two intersections between the radiation circle and the TPD circle for densities between $0.2n_c$ and $0.25n_c$ which actually determine the emission directions of the $3\omega_0/2$ photons (see the $0.23n_c$ curve in Fig. 13). These wave vectors belong to plasmons that can generate $3\omega_0/2$ without propagation. The thin dotted lines are the axes of the new coordinate system at the quarter critical density for an angle of incidence of 45° in which the light wave vector has only one component (x'). This is the natural coordinate system of the $3\omega_0/2$ generation process. At an intensity of 10^{17} W/cm 2 the Landau damping [Eq. (20)] is equal to the homogeneous growth rate on the thin clover-leaf-shaped curve. Electron plasma waves with wave vectors outside of this curve have negative growth rate, i.e., are not amplified by the instability. Inside the curve the Landau damping rate decreases rapidly, so it is negligible there. Consequently, Landau damping is not important for the present conditions. The rough estimation of Landau

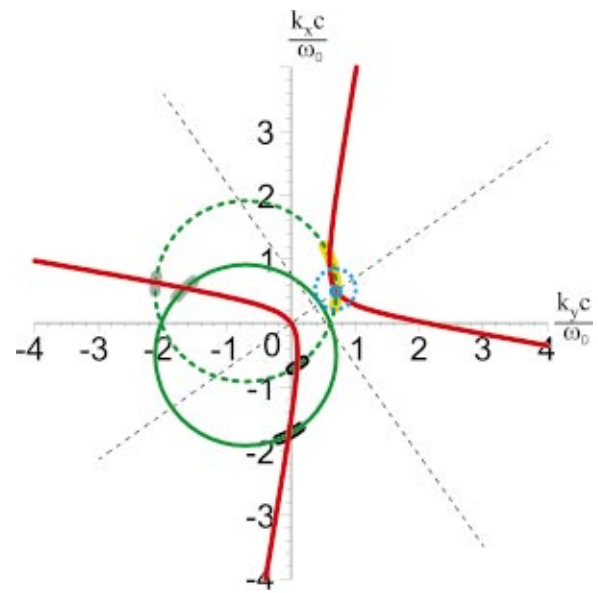


FIG. 14. (Color) k space analysis of the $3\omega_0/2$ generation. The thin dotted axes are the axes of the new coordinate system at the quarter critical in the case of 45° incidence angle. The green thick solid circle is the radiation circle for the coupling of an incident laser photon with a plasmon, while the green thick dashed circle is for the coupling of a laser photon reflected from $n_c/2$ with a plasmon. Along the red thick hyperbola is the growth rate maximal for a homogeneous plasma. The arcs are the intersections between the radiation circles and the hyperbola, representing plasma waves that dominate in the $3\omega_0/2$ production. The light blue curves are SRS generated plasma waves at $0.245n_c$ (smaller) and $0.2n_c$ (larger).

damping at 1 keV temperature gives a criterion for undamped plasma waves $\bar{k}_e < 3.4$ in good agreement with the previous curve. The collisional damping estimated from Eq. (19) is much smaller than the homogeneous growth rate, so we neglect it. This analysis has shown that three-halves harmonic can be generated by TPD plasmons without propagation in the $0.2n_c - 0.25n_c$ density range. However, $3\omega_0/2$ will not be generated everywhere in the k space where it is predicted by the previous analysis, because the analysis does not deliver information about the growth rate, and hence, the amplitude of the plasma waves.

We include the growth rate to account for the plasma wave amplitude and complete theoretical description. In Fig. 14 two radiation circles are shown. While on the green solid circle a $3\omega_0/2$ photon is generated by coupling an incident photon and a plasmon, on the dashed circle a photon reflected from the half critical density is coupled to a plasmon. The estimated value of the resonance absorption is 20%–30%, therefore the reflected light will contribute substantially to the $3\omega_0/2$ production. We expect a significant amplitude of the plasma wave in the k space, where the temporal growth rate is maximal. The red curves are the calculated maximum growth rate hyperbolas Eq. (13). The $3\omega_0/2$ radiation is predominately emitted into the directions given by the intersections of the maximum growth rate hyperbolas and the radiation circles. The black intersections yield a maximum between -20° and -37° where refraction has been taken into account. The dark yellow intersection indicates a maximum between -55° and -71° . Both predictions agree very well with the observed angular depen-

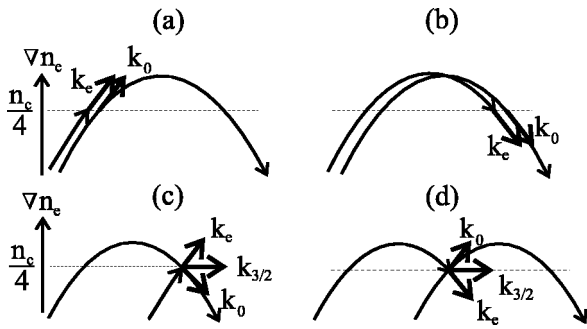


FIG. 15. Coupling geometry of a SRS generated plasmon (wave vector k_e) and a fundamental laser photon (wave vector k_0) to form a $3\omega_0/2$ -photon. In (a) and (b) a collinear coupling is shown, while in (c) and (d) k_e and k_0 are inclined by a certain angle.

dence (see Figs. 8, 9, 10, and 11). The $3\omega_0/2$ is *directly generated* with two incident photons at the lower black intersection ($k_x c/\omega_0 = -1.8; k_y c/\omega_0 = 0$), while it is *indirectly generated* with an incident and a reflected photon at the upper black intersection ($-0.7; 0.1$) and at the dark yellow intersection ($0.2-1.2; 0.6-0.7$). The gray intersections generate back reflected light but no measurement was performed in this direction. It should be noted that the three-halves harmonic radiation propagating into the density gradient in approximately -25° direction experiences maximal resonance absorption as can be seen from Eq. (18). Therefore, the $3\omega_0/2$ emission can be generated only outward propagating in this direction as this analysis also reveals.

SRS may in principle also generate $3\omega_0/2$ radiation. SRS can generate plasmons at the quarter critical density and these plasmons have about the same wave vector as the incident photons. After coupling to an incident laser photon the wave vector of the generated radiation is $2k_0$, but the $3\omega_0/2$ has a wave vector of $\sqrt{8/3}k_0 \approx 1.63k_0$ at this density, Figs. 15(a) and 15(b). Under these conditions the coupling process is not possible. However, coupling is possible in oblique incidence (45° as in the experiment) between the plasmon and a reflected photon as shown in Figs. 15(c) and 15(d). The generated $3\omega_0/2$ photon will have a wave vector perpendicular to the density gradient and will leave the plasma at -71° due to refraction which is the direction of the second measured peak. The results of a more detailed analysis, leading to Eq. (7), are shown in Figs. 13 and 14. The smaller light blue “circle” denotes plasmons generated by SRS at $0.245n_c$ and the larger light blue dashed curve at $0.2n_c$. The smaller curve indicates indirect, while the larger one direct and indirect $3\omega_0/2$ generation. The SRS growth rate reaches its maximum at a density around the quarter critical density Eq. (17). We take the TPD and SRS maximal homogeneous growth rates as a measure of the generated plasma wave amplitudes. Near to the $n_c/4$ both of them reach a value of about $k_0 v_{os}/4$. Thus, it is not possible to decide whether TPD or SRS is responsible for $3\omega_0/2$ production. The momentum conservation is the reason why $3\omega_0/2$ was always created by TPD plasma waves in the long pulse experiments. An angle of incidence of 45° and a very short scale length are required to use SRS plasmons for $3\omega_0/2$ production, which is not the case for long pulses. A possible alternative experiment to

generate three-halves harmonic by SRS is a cylindrical or spherical plasma with a maximal density lower than n_c and two laser pulses from different directions with an angle of 70° between them. Although it remains a challenge to distinguish between SRS and TPD generated light. This distinction may be accomplished for example by scanning the plasmon k space with Thomson scattering or by spectral measurements.

Several factors will modify the previous discussion, such as (1) the plasma inhomogeneity, (2) the high plasma temperature, (3) the validity of plasma wave dispersion relation, (4) the high intensity, (5) the saturation of the instability, and (6) the plasmon propagation.

(1) In an inhomogeneous plasma the maximum growth rate is along the hyperbolas as indicated in Fig. 14, but the value is decreased corresponding to Eq. (15). Therefore, the TPD does not grow if the plasmon’s wave vector is located directly near the axis of the adapted coordinate system (dotted lines in Figs. 13 and 14) which is parallel to \mathbf{k}_0 . However, propagation compensates for that effect.

(2) The higher the plasma temperature the larger is the density range where TPD takes place, and the approximation that the decay takes place exactly at the quarter critical becomes void.³¹ The weight of the k^2 term in the plasma wave dispersion relation grows, which leads to the next point, its validity.

(3) We note that the TPD can occur with a reduced gain *nonresonantly* if only the energy and momentum conservation is fulfilled but not the dispersion relation.³¹ That is, TPD can generate plasmons at a given density and temperature whose wave vectors are not located on the TPD circle in our analysis. This effect modifies the calculated spectrum of the three-halves harmonic radiation also along the radiation circles, which is estimated from this analysis. Nevertheless, the maximal growth is expected along the hyperbolas shown in Fig. 14.

(4) Above 10^{16} W/cm² the dispersion relation is not always satisfied and at relativistic intensities above 10^{18} W/cm² new nonlinear processes start to play a more and more dominant role^{22,23} and the classical theory must be revised. Second order stimulated Raman harmonic generation at the quarter critical leads directly to $3\omega_0/2$ and plasmon production. Two laser photons are simultaneously absorbed and a $3\omega_0/2$ photon and a plasmon are generated. Third order stimulated electromagnetic harmonic generation may create two $3\omega_0/2$ photons from three absorbed laser photons. These nonlinear processes are not important in our measurements, as the intensity was mostly under 10^{18} W/cm², but above this intensity they could contribute to the signal.

(5) Areas in k space with maximal growth determine the emission direction of the $3\omega_0/2$ generation. It is expected that this is slightly modified by saturation because areas with smaller growth rates generate proportionally more $3\omega_0/2$ with than without saturation. We observe with higher laser intensity an increase in the width of both peaks in the angular distribution (Figs. 8, 9, and 11), which may originate from saturation.

(6) The propagation did not play an important role in the long pulse regime, because collisional damping of plasma

waves made the propagation length and thus the change in wave vector negligible. On the other hand, a short propagation distance leads to a large density and wave vector change in the short scale length experiments. Hence, the propagation of plasma waves is an important issue that may influence significantly the plasmon amplitude in the k space. The propagation in the k space is a translation of the plasmon wave vector opposite to the direction of the density gradient (in $-x$ direction) as shown in Fig. 1. During the pulse duration the change in the x component of the normalized wave vector is between 1 and 2 depending on the scale length ($L/\lambda \sim 5.5-2$) starting from an original wave vector of 1, Eq. (10). This effect will elongate the maximum growth region into the $-x$ direction in the k space. Even if the instability growth rate at the lower arc of the black circle in Fig. 14 is very low $3\omega_0/2$ generation may be possible due to plasmon propagation. At the other arm of the hyperbola the propagation mixes the TPD and SRS generated plasma waves. An originally by TPD produced wave will be amplified as it propagates and as its wave vector approaches \mathbf{k}_0 the high frequency hybrid instability—that is a combination of TPD and SRS—and in the vicinity of \mathbf{k}_0 SRS will be the dominant amplification process. Due to the 45° angle of incidence the plasma waves propagate on one arm of the hyperbola and are exposed to the maximal growth continuously during the laser pulse.

These effects will not change the predicted angular distribution but they will affect the relative amplitudes and the spectral characteristics as a function of the observation angle. The possibility that the reflected fundamental will drive an instability is not discussed earlier, but again this will not change the angular distribution. The $3\omega_0/2$ generated in this way will propagate in the direction of the previous peaks.

Detailed spectral measurements were performed in different directions. A redshift and a strongly intensity dependent $3\omega_0/2$ bandwidth were observed in -70° as expected from SRS. A slight blueshift and a weakly intensity dependent bandwidth were measured in -25° in qualitative agreement with the TPD.

Some effects will change the plasma geometry. These are (1) the hole boring, (2) other ponderomotive effects, and (3) the horizontal focus shift.

(1) The light pressure at the turning point pushes the inhomogeneous plasma towards the higher density region. This hole boring effect can lead to ultrahigh plasma acceleration³³ and change the angular distribution of the fundamental,³⁴⁻³⁶ which affects the distribution of the measured harmonics. The depth of the hole and the subsequent defocusing are estimated and the results indicate that both mechanisms have no measurable effect on the angular distribution of reflected fundamental light due to the short pulse duration.^{35,37} For the highest intensities, the angular broadening reaches the angular width caused by diffraction at the end of the laser pulse. This is supported by the angular distribution measurement of the fundamental with an intensity of 6×10^{18} W/cm² plotted in Fig. 7, where the horizontal angular width is determined by the focusing.

(2) The ponderomotive force changes the electron density not only at the reflection point but also below that den-

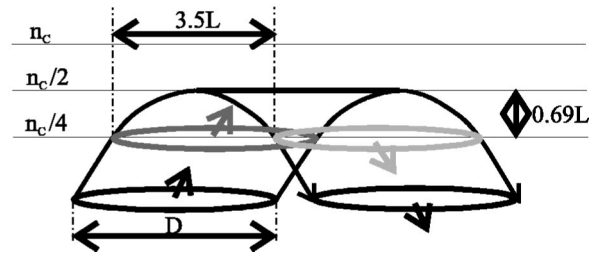


FIG. 16. Horizontal focus shift in the case of 45° incidence angle and an exponential plasma density profile with scale length L and beam diameter D .

sity due to the generated standing wave. This in turn influences the scale length at the quarter critical density.³⁸ The radial ponderomotive force leads to channel formation by pushing electrons away from the middle of the beam. The developed space charge pulls on the ions. These effects are connected to ion motions and require a much longer time scale than the applied 100 fs or need a much longer plasma than the generated one in the experiments.

(3) The incident and reflected beams do not always spatially overlap at the quarter critical density. A horizontal focus shift due to the oblique incidence prevents the beams from overlapping (Fig. 16). Here, we assumed an exponential plasma density profile [$n_0 \times \exp(-x/L)$] with scale length L and a beam diameter D . The horizontal focus shift is approximately $3.5 \times L$. The Rayleigh range is larger than the path length in the plasma from $n_c/4$ to $n_c/2$ and back so we used a constant beam diameter. The two peaks in the $3\omega_0/2$ angular distribution are originating from regions in the k space, where incident and reflected beams coincide, i.e., along the dashed circle in Fig. 14. This overlap and the dashed circle in Fig. 14 and so the indirect $3\omega_0/2$ generation is prevented in a “long” scale length, which is achieved in the experiments (Figs. 10 and 11). The horizontal shift might also explain why for scale lengths longer than 4λ the $3\omega_0/2$ -yield is decreasing and the angular characteristic completely changes.

The -25° peak is larger than the other peak in -70° direction. There are two reasons for this. First, both direct and indirect $3\omega_0/2$ generation mechanisms are important in -25° and only indirect process takes place in -70° . Second, the reflected light has smaller intensity due to resonance absorption, which decreases the efficiency of the indirect process.

The observed decrease in the $2\omega_0$ signal with growing scale length can be explained assuming that the second harmonic is produced at the critical density. The laser light tunnels from the reflection point at $n_c/2$ to n_c , where the $2\omega_0$ is generated. The tunneling distance between $n_c/2$ and n_c increases with the scale length and therefore the fundamental and the $2\omega_0$ intensity are decreasing.

VII. SUMMARY

In conclusion, we presented detailed $3\omega_0/2$ angular distribution and signal measurements. These results made with a femtosecond laser are different from the long pulse results

published earlier and can be explained within the framework of the linear theory. The discussion of the angular distribution was performed applying a k space analysis and the linear model of parametric instabilities. A very good agreement is found between the experimental results and the theoretical predictions. New mechanisms of $3\omega_0/2$ generation have been identified. First, an the indirect generation process involving the incident and the reflected beam, which leads to a double-peaked angular distribution for intermediate scale length. The first higher peak from -20° to -30° direction can be attributed to a coupling between TPD generated plasma waves and the laser light. Second, the origin of the second peak at -70° is due to a combined action of SRS and TPD based plasma wave amplification. Further investigations are needed in order to clarify the role of SRS in the three-halves harmonic production. The well known observation that three-halves harmonic is generated in a preplasma was experimentally confirmed and a model was suggested to explain it. Our measurements show that an inhomogeneous plasma with an electron density scale length larger than approximately $1\ \mu\text{m}$ is required for the $3\omega_0/2$ production thus this light can be used as a simple preplasma diagnostic.

ACKNOWLEDGMENTS

The authors thank P. Gibbon for the useful discussions.

O.R. was supported by a Marie Curie Fellowship of the EC program Improving the Human Research Potential under Contract No. HPMF-CT-2002-01550. This work was supported by the Deutsche Forschungsgemeinschaft (TH 700/1-2).

¹W. L. Kruer, *The Physics of Laser Plasma Interactions* (Addison-Wesley, New York, 1988).

²H. A. Baldis, E. M. Campbell, and W. L. Kruer, in *Handbook of Plasma Physics*, edited by N. M. Rosenbluth and R. G. Sagdeev (Elsevier Science, New York, 1991), Vol. 3, pp. 375–434.

³N. A. Ebrahim, H. A. Baldis, C. Joshi, and R. Benesch, *Phys. Rev. Lett.* **45**, 1179 (1980).

⁴J. Meyer and Y. Zhu, *Phys. Rev. Lett.* **71**, 2915 (1993).

⁵P. E. Young, B. F. Lasinski, W. L. Kruer, E. A. Williams, K. G. Estabrook, E. M. Campbell, R. P. Drake, and H. A. Baldis, *Phys. Rev. Lett.* **61**, 2766 (1988).

⁶C. S. Liu and M. N. Rosenbluth, *Phys. Fluids* **19**, 967 (1976).

⁷See National Technical Information Service Document No. UCRL-50021-77 V1 (B. F. Lasinski and A. B. Langdon, Laser Program Annual Report, Lawrence Livermore National Laboratory UCRL-50021-77, 4-49, 1977). Copies may be ordered from the National Technical Information Service, Springfield, VA 22161.

⁸A. Simon, R. W. Short, E. A. Williams, and T. Dewandre, *Phys. Fluids* **26**, 3107 (1983).

⁹B. B. Afeyan and E. A. Williams, *Phys. Plasmas* **4**, 3827 (1997).

¹⁰D. A. Russell and D. F. DuBois, *Phys. Rev. Lett.* **86**, 428 (2001).

¹¹D. Strickland and G. Mourou, *Opt. Commun.* **56**, 219 (1985).

¹²M. Tabak, J. Hammer, M. E. Glinsky, W. L. Kruer, S. C. Wilks, J. Woodworth, E. M. Campbell, M. D. Perry, and R. J. Mason, *Phys. Plasmas* **1**, 1626 (1994).

¹³C. Rousseau, G. Malka, J. L. Miquel, F. Amiranoff, S. D. Baton, and Ph. Mounaix, *Phys. Rev. Lett.* **74**, 4655 (1995).

¹⁴C. B. Darrow, C. Coverdale, M. D. Perry, W. B. Mori, C. Clayton, K. Marsh, and C. Joshi, *Phys. Rev. Lett.* **69**, 442 (1992).

¹⁵E. Esarey, P. Sprangle, J. Krall, and A. Ting, *IEEE Trans. Plasma Sci.* **24**, 252 (1996).

¹⁶J. D. Kmetec, C. L. Gordon III, J. J. Macklin, B. E. Lemoff, G. S. Brown, and S. E. Harris, *Phys. Rev. Lett.* **68**, 1527 (1992).

¹⁷L. Veisz, W. Theobald, T. Feurer, H. Schillinger, P. Gibbon, R. Sauerbrey, and M. S. Jovanović, *Phys. Plasmas* **9**, 3197 (2002).

¹⁸J. F. Drake, P. K. Kaw, Y. C. Lee, G. Schmidt, C. S. Liu, and M. N. Rosenbluth, *Phys. Fluids* **17**, 778 (1974).

¹⁹D. W. Forslund, J. M. Kindel, and E. L. Lindman, *Phys. Fluids* **18**, 1002 (1975).

²⁰B. B. Afeyan and E. A. Williams, *Phys. Plasmas* **4**, 3803 (1997).

²¹B. B. Afeyan and E. A. Williams, *Phys. Plasmas* **4**, 3845 (1997).

²²H. C. Barr, P. Mason, and D. M. Parr, *Phys. Plasmas* **7**, 2604 (2000).

²³B. Quesnel, P. Mora, J. C. Adam, A. Heron, and G. Laval, *Phys. Plasmas* **4**, 3358 (1997).

²⁴H. A. Baldis and C. J. Walsh, *Phys. Rev. Lett.* **47**, 1658 (1981).

²⁵C. Ziener, G. Stobrawa, H. Schwoerer, I. Uschmann, and R. Sauerbrey, *Rev. Sci. Instrum.* **71**, 3313 (2000).

²⁶I. Uschmann, P. Gibbon, D. Klopfel, T. Feurer, E. Forster, P. Audebert, J.-P. Geindre, J.-C. Gauthier, A. Rousse, and C. Rischel, *Laser Part. Beams* **17**, 671 (1999).

²⁷O. Peyrusse, *Phys. Fluids B* **4**, 2007 (1992).

²⁸J. P. Christiansen, D. E. T. F. Ashby, and K. V. Roberts, *Comput. Phys. Commun.* **7**, 271 (1974).

²⁹S. Bastiani, P. Audebert, J. P. Geindre, Th. Schlegel, J. C. Gauthier, C. Quoix, G. Hamoniaux, G. Grillon, and A. Antonetti, *Phys. Rev. E* **60**, 3439 (1999).

³⁰H. C. Barr, *Proc. VI International Conf. on Plasma Phys.*, Lausanne, 1984, Vol. 3, p. 641.

³¹A. C. Machacek and J. S. Wark, *Phys. Plasmas* **8**, 704 (2001).

³²A. Tarasevitch and D. von der Linde (private communication, 2002).

³³R. Sauerbrey, *Phys. Plasmas* **3**, 4712 (1996).

³⁴S. C. Wilks, W. L. Kruer, M. Tabak, and A. B. Langdon, *Phys. Rev. Lett.* **69**, 1383 (1992).

³⁵T. Feurer, W. Theobald, R. Sauerbrey, I. Uschmann, D. Altenbernd, U. Teubner, P. Gibbon, E. Förster, G. Malka, and J. L. Miquel, *Phys. Rev. E* **56**, 4608 (1997).

³⁶R. J. Kingham, P. Gibbon, W. Theobald, L. Veisz, and R. Sauerbrey, *Phys. Rev. Lett.* **86**, 810 (2001).

³⁷M. Zepf, M. Castro-Colin, D. Chambers *et al.*, *Phys. Plasmas* **3**, 3242 (1996).

³⁸D. T. Attwood, D. W. Sweeney, J. M. Auerbach, and P. H. Y. Lee, *Phys. Rev. Lett.* **40**, 184 (1978).